Quantifying the influence of CO_2 seasonality on future aragonite under-saturation onset

T. P. Sasse[1], B. I. McNeil[1], R. J. Matear[2] and A. Lenton[2]

[1] (Climate Change Research Centre, Kensington Campus, University of New South Wales, Sydney, Australia)

[2] (CSIRO Oceans and Atmosphere National Research Flagship, Hobart, Australia)

Correspondence to: T. P. Sasse (t.sasse@unsw.edu.au)

Abstract

Ocean acidification is a predictable consequence of rising atmospheric carbon dioxide (CO_2), and is highly likely to impact the entire marine ecosystem - from plankton at the base of the food chain to fish at the top. Factors which are expected to be impacted include reproductive health, organism growth and species composition and distribution. Predicting when critical threshold values will be reached is crucial for projecting the future health of marine ecosystems and for marine resources planning and management. The impacts of ocean acidification will be first felt at the seasonal scale, however our understanding how seasonal variability will influence rates of future ocean acidification remains poorly constrained due to current model and data limitations. To address this issue, we first quantified the seasonal cycle of aragonite saturation state utilizing new data-based estimates of global ocean surface dissolved inorganic carbon and alkalinity. This seasonality was then combined with earth system model projections under different emissions scenarios (RCPs 2.6, 4.5 and 8.5) to provide new insights into future aragonite under-saturation onset. Under a high emissions scenario (RCP 8.5), our results suggest accounting for seasonality will bring forward the initial onset of month-long under-saturation by 17±10 years compared to annual-mean estimates, with differences extending up to 35±16 years in the North Pacific due to strong regional seasonality. This earlier onset will result in large-scale under-saturation once atmospheric CO_2 reaches 496ppm in the North Pacific and 511ppm in the Southern Ocean, independent of emission scenario. This work suggests accounting for seasonality is critical to projecting the future impacts of ocean acidification on the marine environment.

1. Introduction

The global ocean currently absorbs about 30% of annual fossil-fuel CO_2 emissions (Le Quéré et al., 2015), and will likely sequester up to 80% of all human-derived CO_2 emissions over the coming centuries (Archer et al., 1997). While this ecosystem service largely mediates the rate of climate change, the immediate impact of this additional CO_2 is a shift in the ocean's chemical composition, resulting in lower pH and carbonate ion (CO_3^{2-}) concentrations - commonly referred to as ocean acidification (OA; Caldeira and Wickett, 2003).

Of great concern is the immediate impact OA is presenting to multiple marine organisms. This includes organisms that require an adequate supply of CO_3^{2-} to form and preserve their calcium carbonate ($CaCO_3$) shells and skeletons (e.g. corals, pteropods and coccolithophorids). Two key parameters for understanding how a change in CO_3^{2-} impacts marine calcifiers are the saturation states for aragonite (Ω_{Ar}; Eq. 1) and calcite (Ω_{Ca}; Eq. 2) - the two main $CaCO_3$ minerals formed by marine calcifiers.

$$\Omega_{Ar} = [Ca^{2+}][CO_3^{2-}]/K^*_{sp(Ar)} \quad (1)$$

$$\Omega_{Ca} = [Ca^{2+}][CO_3^{2-}]/K^*_{sp(Ca)} \quad (2)$$

Here, $[Ca^{2+}]$ and $[CO_3^{2-}]$ represent the concentrations of calcium and carbonate ions respectively, while $K^*_{sp(Ar)}$ and $K^*_{sp(Ca)}$ are the apparent stoichiometric solubility products for aragonite and calcite. Laboratory and mesocosm experiments suggest production and dissolution of biogenic $CaCO_3$ are mainly controlled by seawater Ω levels (Aze et al., 2014; Fabry et al., 2008). These experiments further indicate significant decreases in calcification rates when test species are exposed to Ω levels below their natural range for periods of days to weeks (Chan and Connolly, 2013). Once seawater Ω levels fall below 1, referred to as under-saturation, seawater becomes corrosive to $CaCO_3$ and dissolution can occur. Although experimental studies show detrimental impacts at seawater Ω levels above 1 (e.g., Bednarsek et al., 2012; Fabry et al., 2008), under-saturation is widely regarded as a key threshold value (e.g., Hunt et al., 2008; Orr et al., 2005). Since aragonite is approximately 50% more soluble than calcite, resulting in earlier under-saturation, the focus of this work is on future changes in Ω_{Ar}.

Several previous studies have used Earth System Models (ESM) to predict future annual-mean Ω_{Ar} levels under different CO_2 emission scenarios (Caldeira and Wickett, 2003, 2005; Cao et al., 2007; Kleypas et al., 1999; Orr et al., 2005; Ricke et al., 2013). These annual-mean projections suggest under-saturation will occur in the Southern Ocean and high northern latitudes within the 21st century (e.g. Orr et al., 2005). However, strong natural seasonality in oceanic CO_2 has the potential to significantly alter the onset of future under-saturation, not captured by these approaches.

McNeil and Matear (2008) first demonstrated how strong CO_2 seasonality in the Southern Ocean brings forward the initial onset of month-long aragonite under-saturation conditions by ~30 years relative to annual-mean projections. More recent studies in Australia's Great Barrier Reef (Shaw et al., 2013), Californian coast (Gruber et al., 2012) and Arctic Ocean (Steinacher et al., 2009) further demonstrate the importance of accounting for natural CO_2 seasonality when evaluating future OA levels.

Despite significant efforts over recent years to establish a global carbon measurement network (e.g. the Global Ocean Acidification Observation Network; www.goa-on.org; (Newton et al., 2014)), such a large-scale initiative remains limited by spatial and temporal variability in oceanic CO_2 coupled to the high cost of ship time, resulting in only a limited understanding of CO_2 seasonality throughout the global ocean (Monteiro et al., 2010). This represents a critical gap in our ability to understand and predict the influence of natural variability on the future onset and duration of critical OA levels.

It is important to note that ESMs do provide some insights into regional CO_2 seasonality. However, it has been shown the current generation of ESMs do not accurately capture the observation-based magnitude and/or phase of air-sea CO_2 fluxes in most ocean regions, including the Southern Ocean, North Pacific, Indian Ocean and North Subpolar Atlantic (Ishii et al., 2014; Lenton et al., 2013; Pilcher et al., 2015; Sarma et al., 2013; Schuster et al., 2009). Consequently, these models do not realistically characterize seasonality in Ω_{Ar}.

Here, we use the newly constrained data-based estimates of global ocean surface dissolved inorganic carbon (C_T) and total alkalinity (A_T) of Sasse et al. (2013b) to diagnose monthly Ω_{Ar} distributions for the nominal year of 2000. We then project our monthly observational baselines through to 2100 using decadal trends from an ensemble of Earth System climate models (CMIP5) forced under different emissions scenarios (RCPs 2.6, 4.5 and 8.5). These

results provide new insights into the influence of sea-surface seasonality on the likely onset times for future aragonite under-saturation in the global ocean.

The work presented here expands on the study of McNeil and Matear (2008) with several key improvements: 1) the global CO_2 climatologies of Sasse et al. (2013b) better reflect the latest observations and were derived using a more sophisticated method; 2) we explore the potential for CO_2 disequilibrium to evolve into the future by exploiting CMIP5 model projections; 3) we project the observational baseline using three different emission scenarios (RCP2.5, 4.5 and 8.5); 4) we apply the approach globally rather than the Southern Ocean alone.

2. Diagnosing monthly carbon system distributions

The ocean's inorganic carbon system can be fully constrained by knowing any two parameters within its inorganic carbon constituents - partial pressure of CO_2 (pCO_2), dissolved inorganic carbon (C_T), total alkalinity (A_T) or pH (Dickson et al., 2007). Here we diagnose monthly Ω_{Ar} distributions using the 1°×1° C_T and A_T climatologies of Sasse et al. (2013b) in combination with the World Ocean Atlas 2013 (WOA13) temperature, salinity, and nutrient monthly surface distributions (Objectively analysed decadal averages; Garcia et al., 2014a, b; Locarnini et al., 2013; Zweng et al., 2013). Since the C_T climatologies of Sasse et al. (2013b) were predicted for the nominal year of 2000 (see Sasse et al. (2013b) for details), the Ω_{Ar} values calculated here are also representative of this year.

All calculations were conducted using the total pH scale and carbonic acid dissociation constants of Mehrbach et al (1973) as refitted by Dickson and Millero (1987), K_{SO_4} dissociation constant of Dickson (1990b) and boric acid dissociation constant of Dickson (1990a). Calculations of Ω_{Ar} used the K_{sp} values of Mucci (1983) and [Ca]-salinity relationship of Riley and Tongudai (1967).

To evaluate the realism of our global Ω_{Ar} predictions we compare the network of in-situ Ω_{Ar} values to our corresponding 1°×1° predictions for the same month and location (Fig. 1). In-situ Ω_{Ar} values were calculated using measured A_T and C_T concentrations, where C_T values were first normalised to the year 2000 via observed Revelle factors and assuming constant equilibrium with the atmospheric CO_2 increase (see Sasse et al. (2013b) for details). Our data-based approach is consistent with the general pattern of high Ω_{Ar} values in the tropics which decrease poleward. Our approach also captures well the strong Ω_{Ar} gradients at ~40° North and South and local Ω_{Ar} minimas in equatorial upwelling regions (see Fig. S1 in the

Supplement for monthly Ω_{Ar} distributions). Statistical analysis finds the correlation between the global in-situ values and our corresponding space/month 1°×1° predictions to be 0.98.

We further compare our zonal mean 1°×1° Ω_{Ar} predictions for summer and winter to evaluate the ability of our approach to capture seasonal variability (Fig. 2). The data-based zonal pattern compares well to our general understanding of a strong winter-time minimum in the higher latitudes driven by surface cooling and strong persistent winds that ventilate deep-waters depleted in CO_3^{2-} (McNeil and Matear, 2008). The stronger winter-time minimum in the Northern Hemisphere is consistent with our findings of larger seasonal amplitudes in the North Pacific and Atlantic compared to the Southern Ocean (see Fig. 4).

Our monthly data-based Ω_{Ar} distribution also reconfirms the contemporary ocean surface is supersaturated with respect to aragonite, showing 99.3% of monthly ocean surface waters with Ω_{Ar} levels greater than 1 in the year 2000. The only region where month-long under-saturation was found is in the Arctic Ocean (see Fig. S2), which is consistent with previous data-based (e.g. Mathis and Questel, 2013) and model-based (e.g. Popova et al., 2014) studies.

An independent data-based climatology for monthly ocean surface Ω_{Ar} was presented by Takahashi et al (2014; hereinafter referred to as T14). In their approach, global Ω_{Ar} distributions were calculated for the nominal year of 2005 on a 4°×5° resolution using a combination of interpolated ocean-surface pCO_2 and predicted A_T values via a salinity and nitrate relationship. Estimates in the equatorial Pacific were however omitted due to strong inter-annual variability.

Comparison between T14 and our global Ω_{Ar} values (projected to the year 2005; see Sect. 6) reveals a global correlation of 0.99, with mean Ω_{Ar} values of 2.68 and 2.72 respectively. This good agreement between two independent data-based approaches provides additional confidence in our estimated Ω_{Ar} values. Several key benefits in using our Ω_{Ar} baseline include: 1) better spatial resolution; 2) inclusion of the equatorial Pacific; 3) independent uncertainty estimates in our Ω_{Ar} predictions.

3. Quantifying uncertainties in our Ω_{Ar} predictions

The approach used here to diagnose surface Ω_{Ar} distributions includes both systematic and random sources of error. The main source of random error derives from uncertainties within

the global open-ocean C_T and A_T distributions, which have been estimated to be ±11.8 and ±10.2 μmol kg^{-1} respectively (Sasse et al., 2013b). To quantify the corresponding uncertainty in our calculated Ω_{Ar} values, we applied an independent testing approach using 16,727 mixed-layer C_T and A_T independent predictions of Sasse et al (2013b). In their approach, measurements from each cruise (N=470) and time-series station (N=2) were individually excluded from the empirical model training phase, and then used as an independent dataset to predict C_T and A_T concentrations. Here we employed this dataset to calculated Ω_{Ar} values using both the in-situ C_T and A_T measurements and their corresponding independent predictions. Comparison between these values revealed a global uncertainty in our Ω_{Ar} predictions to be ±0.138 (Residual Standard Error (RSE); Fig. 3a), with summer-time and winter-time RSE values of 0.142 and 0.126 respectively (Fig. 3c,e), indicating no strong seasonal biases.

To evaluate our approach for systematic errors, we analysed the global distribution of residual errors via the independent testing approach described above (Fig. 3b). We further partitioned the residuals by season to evaluate for any temporal bias (see Fig. 3d,f). The global, summer-time and winter-time residual error distributions all followed a near normal distribution with mean residual errors of 0.004, 0.001 and 0.007, respectively, suggesting no strong global or temporal biases in our approach.

To assess for spatial biases, we partitioned the global independent predictions into 14 ocean regions and calculated RSE values (Table 1; see Fig. S3 for regions). Here we find all regional RSE values lie within ±0.04 of the global RSE (0.138), with the exception of the Arctic Ocean, where the RSE value was found to be 0.22 (N=673). In particular, the Southern Ocean is where our approach excels, predicting Ω_{Ar} to within ±0.10 units (N=2923). The small variance in regional RSE values around the global value indicates no spatial bias.

Finally, it is important to acknowledge that uncertainties and biases in the WOA13 objectively analysed products will influence our data-derived Ω_{Ar} distributions. Since error estimates in the WAO13 products remain uncertain, this source of uncertainty cannot be accounted for at this time. However, if we assume errors in WOA13 are uncorrelated and much smaller than errors associated with the carbonate system, then they will not significantly contribute to uncertainty in our calculated Ω_{Ar} values.

4. How large is contemporary seasonal variability?

Seasonal amplitudes were calculated here as the difference between the maximum and minimum monthly Ω_{Ar} values in each 1°×1° grid cell (Fig. 4). From a global open-ocean perspective, seasonality was found to be 0.46±0.25 (1σ), while strong regional mixing/upwelling regimes and/or biological production results in large spatial differences. In the high Northern latitudes (45°N to 70°N) and Southern subtropics (20°S to 45°S) for example, seasonality was found to be strongest at 0.73±0.20 and 0.46±0.14 (1σ) respectively, while seasonality in the equatorial region (20°N to 20°S) was found to be weakest at 0.34±0.21.

From an OA perspective, regions where seasonality is strongest will have the largest implications for the future onset of critical Ω_{Ar} levels. In the tropics for example, where aragonite secreting corals are abundant (Tupper et al., 2011), the relatively weak seasonality will result in little difference between month-long and annual-mean onset for future Ω_{Ar} levels. In the higher latitudes however, where seasonality is largest, the implications for future Ω_{Ar} onset will be much more pronounced.

It must be noted that our seasonal predictions will underestimate some coastal regions where limited data exists. Along the coastal Antarctic continent for example, in-situ data has shown seasonal Ω_{Ar} variability of up to 1.75 (McNeil et al., 2010), which is not captured by our approach.

5. Is seasonality the dominant mode of Ω_{Ar} variability?

Variability in the open-ocean CO_2 system is driven mainly by seasonal and inter-annual variability (IAV), with diurnal variability only playing a significant role in coastal waters (Secretariat of the Convention on Biological Diversity., 2014).

To quantify the relative roles of seasonal and IAV in open-ocean waters, we analysed results from an ensemble of 6 ESM participating in the Coupled Model Inter-comparison 5 project (CMIP5; Table 2). Each model was first re-gridded to a 1°×1° resolution, and then Ω_{Ar} values calculated via the standard CO_2 dissociation constants described in Sect. 2. To constrain the total magnitude of natural variability, we combined the seasonal and IAV signals within each 1°×1° grid cell (Fig. 5a). For IAV, we de-trended annual-mean projections from 2006 through to 2100 under the RCP8.5 emission scenario via a third order polynomial, and then calculated the standard deviation (SD) in the de-trended data (i.e. 95.4% of the year-to-year variance). For seasonality, we used the average seasonal magnitude (maximum minus minimum)

between 2006 and 2016. The relative roles of variability were finally quantified by dividing the individual components by the total variability. We also multiplied these values by 100 to present the relative roles of seasonal variability and IAV as a percentage of the total natural variability (Figs. 5b,c).

This model-based analysis revealed seasonality to be the dominant mode of variability throughout the global open-ocean, accounting for 74±12% (1σ) of total natural variability. From a regional perspective, seasonality is the dominant mode in the higher latitudes, accounting for 84±5% of total variability in the Southern Ocean (South of 30°S) and North Pacific (30°N to 70°N). In the eastern equatorial Pacific however, IAV is the dominant mode of variability, representing up to 70% of total variability (Fig. 5c). With the exception of the central equatorial Pacific, seasonality is the dominant mode of variable across the greater equatorial region (30°S to 30°N), accounting for 67±12% of the total natural variability within this region (Fig. 5b). These results are independent of the emission scenario used to calculate the seasonal and inter-annual components.

Comparison between our data-based Ω_{Ar} seasonal amplitudes (Fig. 4) and model-based total variability (Fig. 5a) reveals a similar spatial pattern in regions where seasonality is the dominant mode (i.e. North Pacific, Southern Ocean and West North Atlantic). Despite this general agreement, we find our data-based seasonal estimates are on average 1.3 times larger than the 2006-2016 model-based mean seasonal amplitudes in the North Atlantic, North Pacific and Southern Ocean (SD=0.5; see Fig. S4). We further compared our databased seasonal amplitudes for the year 2000 to the 2006-2016 mean seasonal amplitudes of the 6 individual ESM output (Table 2). Here we found amplification factors ranged from 0.8 to 2.3, with a mean and standard deviation of 1.3±0.5. This suggests ESMs on average under-predict the oceans seasonal CO_2 cycle by a factor of 1.3 (or 30%).

6. Projecting future Ω_{Ar} levels

Exchange of CO_2 between the ocean and atmosphere is driven by the air-sea gradient in pCO_2. Each year, approximately 70 petagrams of carbon is naturally exchanged at the air-sea interface in both directions (Sarmiento and Gruber, 2002). Comparison between ocean-surface and atmospheric pCO_2 reveals seasonality in the ocean is the dominant driver of this large natural CO_2 flux (Sasse et al., 2013a; Takahashi et al., 2009), which in turn is driven by biological and physical-solubility processes (Sarmiento and Gruber, 2006) - referred to here as the natural cycling of carbon.

If the natural cycling of carbon remained in steady-state throughout the last two centuries, the rate of increase in regionally integrated ocean surface pCO_2 would have roughly tracked the atmospheric CO_2 growth rate over longer timescales (Lenton et al., 2012; Tjiputra et al., 2014). Recent studies have however identified shifts in the oceans natural cycling of carbon due to climate related alterations. For example, decadal-scale trends in ocean surface temperature (Levitus et al., 2005; Lyman et al., 2010) and salinity (Durack and Wijffels, 2010) are influencing both the solubility of CO_2 and ocean circulation pathways, while shifting wind patterns are impacting circulation and seasonal mixing processes, resulting in either enhanced or diminished ventilation of deep waters enriched with C_T and nutrients (e.g. Le Quéré et al., 2007; Lenton et al., 2009).

Added to this climate-mediated change in oceanic CO_2 uptake, the air-sea exchange of CO_2 is a slow process (approximately 1 year equilibration time), where local physical and biological processes can cause the ocean to deviate from atmospheric CO_2. This creates a difference between the atmospheric and ocean surface pCO_2 (disequilibrium). Further, as atmospheric CO_2 increases, ocean processes can cause the ocean to lag the atmospheric increase and the disequilibrium term to increase with time (McNeil and Matear, 2013). For example, in the polar regions, short residence times of surface waters and the ventilation of old CO_2-rich deep waters creates an increasing CO_2 disequilibrium, resulting in a growing difference between atmospheric and surface ocean CO_2 over time.

To account for the effects of future climate change and increasing CO_2 disequilibrium described above, we projected our data-based CO_2 climatologies using results from an ensemble of 6 ESM (Table 2). In this approach, decadal trends in C_T, A_T, temperature and salinity were combined with the monthly data-based C_T and A_T and WOA13 temperature and salinity products. Monthly Ω_{Ar} values were then calculated using the standard CO_2 dissociation constants presented in Sect. 2.

We projected our CO_2 base-lines using ESM results forced under several different Representative Concentration Pathways (RCP8.5, 4.5 and 2.6). Here, RCP8.5 is a *business-as-usual* scenario with little mitigation and peak CO_2 concentrations at 935 parts per million (ppm) in the year 2100; RCP4.5 is a scenario where emissions peak in mid-century and are then slowly reduced, resulting in a peak CO_2 concentration of 538ppm by 2100; finally, RCP2.6 is a *best-case* scenario were emissions are dramatically reduced in the near future to

276 the point where more CO_2 is absorbed by the ocean and terrestrial biosphere than emitted by
277 human activities (Meinshausen et al., 2011).

278 It should be emphasised that the observation-based CO_2 climatologies of Sasse et al (2013b)
279 have been shown to accurately reconstruct the global pattern of present-day ocean surface
280 CO_2 variability. However, for this study we assume constant seasonality from our baseline
281 CO_2 climatologies throughout the 21st century. Although this assumption is likely adequate
282 for short temporal projections (<10years), a recent evaluation of 10 ESM suggests large
283 changes in mixing, biological production and CO_2 solubility will occur within the 21st century
284 (Bopp et al., 2013). By projecting our base-line climatologies using decadal trends from ESM
285 we implicitly capture the decadal response to these changes, however, any potential shift in
286 the phase and magnitude of CO_2 seasonality are not explored in our approach.

287 Given the limitations in the current generation of ESM in capturing seasonality in air-sea CO_2
288 flux and/or ocean surface pCO_2 in many important regions (Ishii et al., 2014; Lenton et al.,
289 2013; Pilcher et al., 2015; Sarma et al., 2013; Schuster et al., 2009), their ability to
290 realistically project future changes in CO_2 seasonality is questionable. We therefore do not
291 account for any change in CO_2 seasonality in the current study. Once models evolve to a point
292 where seasonality of the carbon system is well-represented, potential future changes to
293 seasonality will need to be explored in future studies.

294 As a first step to assess the sensitivity of future Ω_{Ar} predictions to shifts in oceanic CO_2
295 seasonality, we applied the following approach to model output from 6 EMS (Table 2).
296 Seasonal cycles in C_T, A_T, temperature and salinity were first averaged over the decades 2006
297 through 2015 and 2091 through 2100 in each 1°×1° grid cell. Annual-mean values from the
298 2091-2100 mean seasonal cycle were then added to the 2006-2015 mean seasonal cycles,
299 thereby shifting the earlier seasonal cycle to typical values of the years 2090-2100. Finally,
300 seasonal Ω_{Ar} values were computed using both the mean 2091-2100 and shifted 2006-2015
301 C_T, A_T, Temperature and Salinity values. Comparing the seasonal amplitudes in Ω_{Ar} found
302 shifted values were on average 5.4% larger than the 2091-2100 average model output for the
303 global open-ocean (sd = 48%), with individual model differences ranging from -0.4% to
304 19.1%. This suggests our data-based Ω_{Ar} amplitudes are on average 5.4% larger than
305 expected if changes in C_T, A_T, temperature and salinity seasonality were additionally taken
306 into account.

307 **7. Quantifying the onset of aragonite under-saturation**

When strong natural carbon seasonality is combined with a long-term trend, the onset and exposure times of biological thresholds are influenced. To illustrate this point, we present Ω_{Ar} projections under the *business-as-usual* scenario (RCP8.5) at two 1°x1° sites in the North Atlantic and Southern Ocean which are somewhat representative of the larger region (Fig. 6). At the North Atlantic site, strong seasonality was found to bring forward the initial onset (time a in Fig. 6a) of aragonite under-saturation by 27 years relative to the annual-mean (time b; Fig. 6a), while weaker variability at the Southern Ocean site brings forward under-saturation by 8 years (Fig. 6b). It's important to emphasize that monthly under-saturation conditions starts at time a, and then eventually extends to be permanent over all months (time c). As much as seasonality brings forward the initial onset of under-saturation, it also delays the permanent onset (Fig. 6). At the Southern Ocean site for example, seasonality delays the permanent onset by ~15 years. In the context of ocean acidification impacts, monthly exposure times are important, since laboratory experiments show even short exposure times (i.e. hours to days) can result in significant implications to the health and well-being of the test species (Chan and Connolly, 2013).

7.1 Future Ω_{Ar} levels under RCP8.5

Under the *business-as-usual* scenario (RCP8.5), our results show annual-mean aragonite under-saturation will occur by the year 2086±9 (1σ) in the North Pacific and North Atlantic, 2074±12 in the Southern Ocean, while tropical and temperate regions (~40°S to ~40°N) will remain super-saturated beyond the year 2100 (Fig. 7a). When seasonality is considered, the initial month-long onset precedes annual-mean estimates by a global average of 17±10 years (1σ) under the RCP8.5 scenario (70°N to 70°S; Figs. 7b-c). In the North Pacific and North Atlantic, where seasonality is strongest, month-long under-saturation is brought forward by 36±16 and 19±6 years respectively (Fig. 7c).

In the Southern Ocean (South of 60°S), our results show month-long aragonite under-saturation will first occur as early as the year 2030, or when atmospheric CO_2 concentrations reach ~450ppm. While this is consistent with projections by McNeil and Matear (2008) under the IPCC IS92a scenario, our results show seasonality will delay the onset of annual-mean under-saturation by 14±7 years, which is half the delay time found by McNeil and Matear (2008). This difference likely reflects the faster rate of change in atmospheric CO_2 under RCP8.5 compared to IPCC IS92a, while differences in seasonality found by the two approaches is likely a secondary factor.

Wide-spread onset of permanent Ω_{Ar} under-saturation is only found in the Southern Ocean and Arctic Ocean by the year 2100 (see Fig. S5). In the Southern Ocean, the average time difference between annual-mean and permanent onset is 13.0±5.3 years, which is similar to the time difference found between annual-mean and month-long onset at the same locations (13.0±5.9 years). Despite these similar basin-wide time difference values, the correlation coefficient was found to be 0.31, indicating significant spatial differences. This reflects the non-symmetrical nature of seasonal Ω_{Ar} cycles in some regions of the Southern Ocean, as observed in Fig. 6b, which further highlights the importance of accounting for seasonal processes.

Early aragonite under-saturation is of particular concern for the many important calcifying organisms that inhabit the higher latitudes. Pteropods for example, are a zooplankton species that forms aragonite shells to provide ballast for vertical migration in search of food and breeding. In the Southern Ocean, pteropods have been found to represent up to 30% of total zooplankton (Hunt et al., 2008), and are themselves important prey for larger zooplankton, as well as many fish and bird species (Hunt et al., 2008; Karnovsky et al., 2008). From a biogeochemical perspective, pteropods account for at least 12% of the global $CaCO_3$ flux into the ocean interior (Berner and Honjo, 1981). When pteropods sink to depths at which $\Omega_{Ar} = 1$, known as the saturation horizon or lysocline, field studies show significant dissolution occurs (Hunt et al., 2008). As more anthropogenic CO_2 enters the ocean system, the aragonite saturation horizon will approach the upper ocean until the surface waters become permanently under-saturated. Decade(s) before this occurs however, seasonality will expose calcifying organisms to detrimental month-long under-saturation conditions, causing unknown implications for the wider food web.

7.2 Future Ω_{Ar} levels under RCP 4.5 and 2.6

In the previous section we presented results under the RCP8.5 scenario. We now explore how lower emission scenarios influence future onset of aragonite under-saturation. We consider our Ω_{Ar} projections under RCP4.5, 2.6 and their behaviour relative to RCP8.5 (Table 3 and Fig. 8). In the North Pacific, we find month-long aragonite under-saturation occurs by the year 2057±24 and 2040±15 under RCP4.5 and 8.5, respectively. Despite this difference in onset year, atmospheric CO_2 concentrations at time of onset are consistent at 492±45ppm and 501±60ppm for RCP4.5 and 8.5 respectively, with a correlation co-efficient of 0.75 (Table 3). As expected, this suggests under-saturation onset is highly dependent on the atmospheric CO_2

concentration, where we find large scale under-saturation in the North Pacific once atmospheric CO_2 reaches 496ppm (mean of RCP4.5 and 8.5). Similarly, our results suggest wide spread aragonite under-saturation will occur when atmospheric CO_2 reaches concentrations of 517ppm in the North Atlantic and 511ppm in the Southern Ocean.

Under RCP2.6, whereby emissions are drastically reduced in the near future, our results show very sparse under-saturation onset in the major ocean basins by the year 2100 (Fig. 8). When compared to projections under RCP8.5, we find a 92.6% (or 83.6×10^6 km^2) reduction in global open-ocean surface waters exposed to at least month-long aragonite under-saturation within the 21st century. Regionally, this reduction increases to 98.9% (62.8×10^6 km^2), 92.8% (9.16×10^6 km^2) and 99.2% (6.8×10^6 km^2) in the Southern Ocean, North Pacific and North Atlantic respectively. This result highlights the potential difference humanity can make by reducing CO_2 emissions in the near future.

To further probe the influence of a lower emission scenario on future OA onset, we compare the time difference between month-long and annual-mean aragonite under-saturation onset under RCP8.5 and RCP4.5 at 457 1°×1° grid cell locations in the Southern Ocean (Figs. 8a and 7b). Here we find the average onset for month-long under-saturation occurs by the year 2048 under RCP8.5, and 2073 under RCP4.5. Despite the lower emission scenario delaying the initial onset, we find the time difference between month-long and annual mean onset is 18 years longer under RCP4.5 compared to RCP8.5 (i.e. 14 years under RCP8.5 and 32 years under RCP4.5). This longer time delay under RCP4.5 emphasizes that seasonality becomes even more important when projecting future OA levels under a slower emissions scenario.

8 How does seasonality influence the geographical extent of aragonite under-saturation?

Accounting for seasonality also presents significant implications for the spatial pattern of future aragonite under-saturation. Here we refer to regions where seasonality induces at least month-long under-saturation conditions while annual-mean Ω_{Ar} projections remain super-saturated throughout the 21st century. By the year 2100, the latitudinal extent of ocean surface exposed to at least month-long aragonite under-saturation will have shifted equatorward by ~3.5° degrees relative to the extent of annual-mean estimates under the RCP8.5 scenario (Fig. 9). This extension translates to ~23×10^6 km^2 of ocean surface (or 6.8% of total open-ocean area) exposed to at least month-long aragonite under-saturation by the year 2100 under the *business-as-usual* scenario (RCP8.5). This expansion of corrosive aragonite conditions is

likely to impact multiple marine calcifying organisms living within these regions much earlier than anticipated under previous annual-mean projections (e.g. Orr et al., 2005). Pteropods for example, represent up to 30% of total zooplankton species around the Prince Edward Islands (PEI; Fig. 9; Hunt et al., 2008), if these stocks deplete under future OA levels, the many other animals that rely on pteropods as a source of food will also be detrimentally impacted.

9 Conclusion

Ocean acidification is a global issue which is likely to impact the entire marine ecosystem - from plankton at the base of the food chain to fish at the top. Of particular concern is the decreasing concentration of CO_3^{2-} ions, which lowers the saturation states of $CaCO_3$ minerals (Ω_{Ar} and Ω_{Ca}) and results in detrimental seawater conditions for marine calcifiers (e.g. pteropods and corals; Aze et al., 2014; Fabry et al., 2008). Predicting when critical Ω_{Ar} threshold values will be reached is crucial for projecting the future health of marine ecosystems and for marine resources planning and management. Here we have assessed how seasonality in oceanic CO_2 will influence the future onset of Ω_{Ar} under-saturation.

The influence of seasonality was evaluated by comparing the difference in future month-long and annual-mean Ω_{Ar} under-saturation onset. Our results suggest seasonality brings forward the initial onset of month-long under-saturation by 17±10 years compared to annual mean estimates under RCP8.5, with differences extending up to 35±17 years in the North Pacific due to strong regional seasonality. Our results further show large-scale under-saturation once atmospheric CO_2 reaches 496ppm in the North Pacific, 517ppm in the North Atlantic and 511ppm in the Southern Ocean, independent of emission scenario. It's important to note that seasonality in these regions was also found to be the dominate mode of variability, accounting for 84±5% of total model-based variability in the Southern Ocean (South of 30°S) and North Pacific (30°N to 70°N). This suggests IAV will not significantly alter onset times found in this study.

Under lower emission scenarios, the average time difference between month-long and annual-mean aragonite under-saturation onset increased from 14 years under RCP8.5 to 32 years under RCP4.5 in the Southern Ocean. This longer time difference under a lower emissions scenario emphasizes the importance of accounting for seasonality when projecting future OA levels under a slower emissions scenario. The spatial extent of Ω_{Ar} under-saturation is also drastically reduced under a lower emission scenario. When comparing projections under

RCP2.6 to RCP8.5 for example, our results show a 92.6% (or 83.6×10^6 km^2) reduction in open-ocean surface water exposed to Ω_{Ar} under-saturation by the year 2100, emphasising the importance of mitigating CO_2 emissions in the near future.

Seasonality also influences the spatial pattern of future Ω_{Ar} under-saturation. Here we found the latitudinal extent of month-long under-saturation extended equatorward by a global average of 3.5° (or 23×10^6 km^2) compared to annual-mean projections under RCP8.5. From a biogeochemical perspective, this is particularly concerning given the regions of expansion from the poles (~40° to 50° South and North) are known as important hot-spots for $CaCO_3$ export (Sarmiento and Gruber, 2006).

Finally, the implication of our results are not limited to the higher latitudes, strong Ω_{Ar} seasonality in some subtropical regions (30°S-30°N; see Fig. 4) will likely bring forward the onset of lower Ω_{Ar} waters by similar temporal periods. Since these regions are rich with sensitive calcifying coral reef ecosystems, considering the influence of seasonality is important when estimating future OA levels and their impacts in these regions.

Acknowledgements

T.P. Sasse would like to acknowledge the funding support from the CSIRO carbon cluster. A. Lenton and R.J. Matear would like to acknowledge the funding support of CSIRO Oceans and Atmosphere and the Australian Climate Change Science Program.

References

Archer, D., Kheshgi, H., Maier, and Reimer, E. (1997), Multiple timescales for neutralization of fossil fuel CO_2, Geophys. Res. Lett., 24, 405-408, DOI: 10.1029/97gl00168

Aumont, O., and Bopp, L. (2006), Globalizing results from ocean in situ iron fertilization studies, Global Biogeochemical Cycles, 20, GB2017, DOI: 10.1029/2005gb002591

Secretariat of the Convention on Biological Diversity (2014), An Updated Synthesis of the Impacts of Ocean Acidification on Marine Biodiversity, (Eds: Hennige, S., Roberts, J. M., and Williamson, P.), Montreal, Technical Series no. 75, 99 pp.

Bednarsek, N., Tarling, G. A., Bakker, D. C. E., Fielding, S., Jones, E. M., Venables, H. J., Ward, P., Kuzirian, A., Leze, B., Feely, R. A., and Murphy, E. J. (2012), Extensive dissolution of live pteropods in the Southern Ocean, Nature Geosci, 5, 881-885, DOI: 10.1038/ngeo1635

Berner, R. A., and Honjo, S. (1981), Pelagic Sedimentation of Aragonite: Its Geochemical Significance, Science, 211, 940-942, DOI: 10.1126/science.211.4485.940

Bopp, L., Resplandy, L., Orr, J. C., Doney, S. C., Dunne, J. P., Gehlen, M., Halloran, P., Heinze, C., Ilyina, T., Séférian, R., Tjiputra, J., and Vichi, M. (2013), Multiple stressors of ocean ecosystems in the 21st century: projections with CMIP5 models, Biogeosciences, 10, 6225-6245, DOI: 10.5194/bg-10-6225-2013

Caldeira, K., and Wickett, M. E. (2003), Oceanography: Anthropogenic carbon and ocean pH, Nature, 425, 365-365, DOI: 10.1038/425365a

Caldeira, K., and Wickett, M. E. (2005), Ocean model predictions of chemistry changes from carbon dioxide emissions to the atmosphere and ocean, Journal of Geophysical Research: Oceans, 110, C09S04, DOI: 10.1029/2004JC002671

Cao, L., Caldeira, K., and Jain, A. K. (2007), Effects of carbon dioxide and climate change on ocean acidification and carbonate mineral saturation, Geophys. Res. Lett., 34, L05607, DOI: 10.1029/2006gl028605

Chan, N. C. S., and Connolly, S. R. (2013), Sensitivity of coral calcification to ocean acidification: a meta-analysis, Global Change Biology, 19, 282-290, DOI: 10.1111/gcb.12011

Dickson, A. G., and Millero, F. J. (1987), A comparison of the equilibrium constants for the dissociation of carbonic acid in seawater media, Deep Sea Research Part A. Oceanographic Research Papers, 34, 1733-1743, DOI: 10.1016/0198-0149(87)90021-5

Dickson, A. G. (1990a), Thermodynamics of the dissociation of boric acid in synthetic seawater from 273.15 to 318.15 K, Deep Sea Research Part A. Oceanographic Research Papers, 37, 755-766, DOI: 10.1016/0198-0149(90)90004-F

Dickson, A. G. (1990b), Standard potential of the reaction: AgCl(s) + 1/2H_2(g) = Ag(s) + HCl(aq), and and the standard acidity constant of the ion HSO_4^- in synthetic sea water from 273.15 to 318.15 K, The Journal of Chemical Thermodynamics, 22, 113-127, DOI: 10.1016/0021-9614(90)90074-Z

Dickson, A. G., Sabine, C. L., and Christian, J. R. (Eds.) (2007), Guide to best practices for ocean CO_2 measurements, PICES Special Publication 3, 191 pp.

Dunne, J. P., John, J. G., Shevliakova, E., Stouffer, R. J., Krasting, J. P., Malyshev, S. L., Milly, P. C. D., Sentman, L. T., Adcroft, A. J., Cooke, W., Dunne, K. A., Griffies, S. M., Hallberg, R. W., Harrison, M. J., Levy, H., Wittenberg, A. T., Phillips, P. J., and Zadeh, N. (2013), GFDL's ESM2 Global Coupled Climate–Carbon Earth System Models. Part II: Carbon System Formulation and Baseline Simulation Characteristics*, Journal of Climate, 26, 2247-2267, DOI: 10.1175/JCLI-D-12-00150.1

Durack, P. J., and Wijffels, S. E. (2010), Fifty-Year Trends in Global Ocean Salinities and Their Relationship to Broad-Scale Warming, Journal of Climate, 23, 4342-4362, DOI: 10.1175/2010jcli3377.1

Fabry, V. J., Seibel, B. A., Feely, R. A., and Orr, J. C. (2008), Impacts of ocean acidification on marine fauna and ecosystem processes, ICES Journal of Marine Science / Journal du Conseil, 65, 414-432, DOI: 10.1093/icesjms/fsn048

Garcia, H. E., Locarnini, R. A., Boyer, T. P., Antonov, J. I., Baranova, O. K., Zweng, M. M., Reagan, J. R., and Johnson, D. R. (2014a), World Ocean Atlas 2013, Volume 3: Dissolved Oxygen, Apparent Oxygen Utilization, and Oxygen Saturation, in, edited by: Levitus, S., and Mishonov, A., NOAA Atlas NESDIS 75, 27 pp.

Garcia, H. E., Locarnini, R. A., Boyer, T. P., Antonov, J. I., Baranova, O. K., Zweng, M. M., Reagan, J. R., and Johnson, D. R. (2014b), World Ocean Atlas 2013, Volume 4: Dissolved Inorganic Nutrients (phosphate, nitrate, silicate), in, edited by: Levitus, S., and Mishonov, A., NOAA Atlas NESDIS 76, 25, 25 pp.

Gruber, N., Hauri, C., Lachkar, Z., Loher, D., Frölicher, T. L., and Plattner, G.-K. (2012), Rapid Progression of Ocean Acidification in the California Current System, Science, 337, 220-223, DOI: 10.1126/science.1216773

Hunt, B. P. V., Pakhomov, E. A., Hosie, G. W., Siegel, V., Ward, P., and Bernard, K. (2008), Pteropods in Southern Ocean ecosystems, Progress In Oceanography, 78, 193-221, DOI: 10.1016/j.pocean.2008.06.001

Ilyina, T., Six, K. D., Segschneider, J., Maier-Reimer, E., Li, H., and Núñez-Riboni, I. (2013), Global ocean biogeochemistry model HAMOCC: Model architecture and performance as component of the MPI-Earth system model in different CMIP5 experimental realizations, Journal of Advances in Modeling Earth Systems, 5, 287-315, DOI: 10.1029/2012MS000178

Ishii, M., Feely, R. A., Rodgers, K. B., Park, G. H., Wanninkhof, R., Sasano, D., Sugimoto, H., Cosca, C. E., Nakaoka, S., Telszewski, M., Nojiri, Y., Mikaloff Fletcher, S. E., Niwa, Y., Patra, P. K., Valsala, V., Nakano, H., Lima, I., Doney, S. C., Buitenhuis, E. T., Aumont, O., Dunne, J. P., Lenton, A., and Takahashi, T. (2014), Air–sea CO_2 flux in the Pacific Ocean for the period 1990-2009, Biogeosciences, 11, 709-734, DOI: 10.5194/bg-11-709-2014

Karnovsky, N. J., Hobson, K. A., Iverson, S., and Hunt, G. L. J. (2008), Seasonal changes in diets of seabirds in the North Water Polynya: a multiple-indicator approach, Marine Ecology Progress Series, 357, 291-299, DOI: 10.3354/meps07295

Kleypas, J. A., Buddemeier, R. W., Archer, D., Gattuso, J.-P., Langdon, C., and Opdyke, B. N. (1999), Geochemical consequences of increased atmospheric carbon dioxide on coral reefs, Science, 284, 118-120, DOI: 10.1126/science.284.5411.118

Le Quéré, C., Rödenbeck, C., Buitenhuis, E. T., Conway, T. J., Langenfelds, R., Gomez, A., Labuschagne, C., Ramonet, M., Nakazawa, T., Metzl, N., Gillett, N., and Heimann, M. (2007), Saturation of the Southern Ocean CO_2 Sink Due to Recent Climate Change, Science, 316, 1735-1738, DOI: 10.1126/science.1136188

Le Quéré, C., Moriarty, R., Andrew, R. M., Peters, G. P., Ciais, P., Friedlingstein, P., Jones, S. D., Sitch, S., Tans, P., Arneth, A., Boden, T. A., Bopp, L., Bozec, Y., Canadell, J. G., Chini, L. P., Chevallier, F., Cosca, C. E., Harris, I., Hoppema, M., Houghton, R. A., House, J. I., Jain, A. K., Johannessen, T., Kato, E., Keeling, R. F., Kitidis, V., Klein Goldewijk, K., Koven, C., Landa, C. S., Landschützer, P., Lenton, A., Lima, I. D., Marland, G., Mathis, J. T., Metzl, N., Nojiri, Y., Olsen, A., Ono, T., Peng, S., Peters, W., Pfeil, B., Poulter, B., Raupach, M. R., Regnier, P., Rödenbeck, C., Saito, S., Salisbury, J. E., Schuster, U., Schwinger, J., Séférian, R., Segschneider, J., Steinhoff, T., Stocker, B. D., Sutton, A. J., Takahashi, T., Tilbrook, B., van der Werf, G. R., Viovy, N., Wang, Y. P., Wanninkhof, R., Wiltshire, A., and Zeng, N. (2015), Global carbon budget 2014, Earth Syst. Sci. Data, 7, 47-85, DOI: 10.5194/essd-7-47-2015

Lenton, A., Codron, F., Bopp, L., Metzl, N., Cadule, P., Tagliabue, A., and Le Sommer, J. (2009), Stratospheric ozone depletion reduces ocean carbon uptake and enhances ocean acidification, Geophys. Res. Lett., 36, L12606, DOI: 10.1029/2009gl038227

Lenton, A., Metzl, N., Takahashi, T., Kuchinke, M., Matear, R. J., Roy, T., Sutherland, S. C., Sweeney, C., and Tilbrook, B. (2012), The observed evolution of oceanic pCO_2 and its drivers over the last two decades, Global Biogeochem. Cycles, 26, GB2021, DOI: 10.1029/2011gb004095

Lenton, A., Tilbrook, B., Law, R. M., Bakker, D., Doney, S. C., Gruber, N., Ishii, M., Hoppema, M., Lovenduski, N. S., Matear, R. J., McNeil, B. I., Metzl, N., Mikaloff Fletcher, S. E., Monteiro, P. M. S., Rödenbeck, C., Sweeney, C., and Takahashi, T. (2013), Sea–air CO_2 fluxes in the Southern Ocean for the period 1990-2009, Biogeosciences, 10, 4037-4054, DOI: 10.5194/bg-10-4037-2013

Levitus, S., Antonov, J., and Boyer, T. (2005), Warming of the world ocean, 1955-2003, Geophys. Res. Lett., 32, L02604, DOI: 10.1029/2004gl021592

Locarnini, R. A., Mishonov, A. V., Antonov, J. I., Boyer, T. P., Garcia, H. E., Baranova, O. K., Zweng, M. M., Paver, C. R., Reagan, J. R., Johnson, D. R., Hamilton, M., and Seidov, D. (2013),

World Ocean Atlas 2013, Volume 1: Temperature, in, edited by: S. Levitus, E., and A. Mishonov, T. E., NOAA Atlas NESDIS 73, 40 pp.

Lyman, J. M., Good, S. A., Gouretski, V. V., Ishii, M., Johnson, G. C., Palmer, M. D., Smith, D. M., and Willis, J. K. (2010), Robust warming of the global upper ocean, Nature, 465, 334-337, DOI: 10.1038/nature09043

Mathis, J. T., and Questel, J. M. (2013), Assessing seasonal changes in carbonate parameters across small spatial gradients in the Northeastern Chukchi Sea, Continental Shelf Research, 67, 42-51, DOI: 10.1016/j.csr.2013.04.041

McNeil, B. I., and Matear, R. J. (2008), Southern Ocean acidification: A tipping point at 450-ppm atmospheric CO_2, Proceedings of the National Academy of Sciences, 105, 18860-18864, DOI: 10.1073/pnas.0806318105

McNeil, B. I., Tagliabue, A., and Sweeney, C. (2010), A multi-decadal delay in the onset of corrosive 'acidified' waters in the Ross Sea of Antarctica due to strong air-sea CO_2 disequilibrium, Geophys. Res. Lett., 37, L19607, DOI: 10.1029/2010gl044597

McNeil, B. I., and Matear, R. J. (2013), The non-steady state oceanic CO_2 signal: its importance, magnitude and a novel way to detect it, Biogeosciences, 10, 2219-2228, DOI: 10.5194/bg-10-2219-2013

Mehrbach, C., Culberson, C. H., Hawley, J. E., and Pytkowicz, R. M. (1973), Measurement of the Apparent Dissociation Constants of Carbonic Acid in Seawater at Atmospheric Pressure, Limnology and Oceanography, 18, 897-907

Meinshausen, M., Smith, S. J., Calvin, K., Daniel, J. S., Kainuma, M. L. T., Lamarque, J. F., Matsumoto, K., Montzka, S. A., Raper, S. C. B., Riahi, K., Thomson, A., Velders, G. J. M., and Vuuren, D. P. P. (2011), The RCP greenhouse gas concentrations and their extensions from 1765 to 2300, Climatic Change, 109, 213-241, DOI: 10.1007/s10584-011-0156-z

Monteiro, P., Schuster, U., Hood, M., Lenton, A., Metzl, N., Olsen, A., Rogers, K., Sabine, C., Takahashi, T., Tilbrook, B., Yoder, J., Wanninkhof, R., and Watson, A. J.: A Global Sea Surface Carbon Observing System: Assessment of Changing Sea Surface CO_2 and Air-Sea CO_2 Fluxes, Proceedings of OceanObs'09: Sustained Ocean Observations and Information for Society (Vol. 2), Venice, Italy, 21-25 September 2009, 2010.

Mucci, A. (1983), The solubility of calcite and aragonite in seawater at various salinities, temperatures, and one atmosphere total pressure, American Journal of Science, 283, 780-799, DOI: 10.2475/ajs.283.7.780

Newton, J. A., Feely, R. A., Jewett, E. B., Williamson, P., and Mathis, J. (2014), Global Ocean Acidification Observing Network: Requirements and Governance Plan, First ed., 60 pp.

637 Orr, J. C., Fabry, V. J., Aumont, O., Bopp, L., Doney, S. C., Feely, R. A., Gnanadesikan, A., Gruber,
638 N., Ishida, A., Joos, F., Key, R. M., Lindsay, K., Maier-Reimer, E., Matear, R., Monfray, P., Mouchet,
639 A., Najjar, R. G., Plattner, G.-K., Rodgers, K. B., Sabine, C. L., Sarmiento, J. L., Schlitzer, R., Slater,
640 R. D., Totterdell, I. J., Weirig, M.-F., Yamanaka, Y., and Yool, A. (2005), Anthropogenic ocean
641 acidification over the twenty-first century and its impact on calcifying organisms, Nature, 437, 681-
642 686, DOI: 10.1038/nature04095

643
644 Palmer, J. R., and Totterdell, I. J. (2001), Production and export in a global ocean ecosystem model,
645 Deep Sea Research Part I: Oceanographic Research Papers, 48, 1169-1198, DOI: 10.1016/S0967-
646 0637(00)00080-7

647
648 Pilcher, D. J., Brody, S. R., Johnson, L., and Bronselaer, B. (2015), Assessing the abilities of CMIP5
649 models to represent the seasonal cycle of surface ocean pCO_2, Journal of Geophysical Research:
650 Oceans, 120, 4625-4637, DOI: 10.1002/2015JC010759

651
652 Popova, E. E., Yool, A., Aksenov, Y., Coward, A. C., and Anderson, T. R. (2014), Regional
653 variability of acidification in the Arctic: a sea of contrasts, Biogeosciences, 11, 293-308, DOI:
654 10.5194/bg-11-293-2014

655
656 Ricke, K. L., Orr, J. C., Schneider, K., and Caldeira, K. (2013), Risks to coral reefs from ocean
657 carbonate chemistry changes in recent earth system model projections, Environmental Research
658 Letters, 8, 034003, DOI: 10.1088/1748-9326/8/3/034003

659
660 Riley, J. P., and Tongudai, M. (1967), The major cation/chlorinity ratios in sea water, Chemical
661 Geology, 2, 263-269, DOI: 10.1016/0009-2541(67)90026-5

662
663 Sarma, V. V. S. S., Lenton, A., Law, R. M., Metzl, N., Patra, P. K., Doney, S., Lima, I. D.,
664 Dlugokencky, E., Ramonet, M., and Valsala, V. (2013), Sea–air CO_2 fluxes in the Indian Ocean
665 between 1990 and 2009, Biogeosciences, 10, 7035-7052, DOI: 10.5194/bg-10-7035-2013

666
667 Sarmiento, J. L., and Gruber, N. (2002), Sinks for Anthropogenic Carbon, Physics Today, 55, 30-36,
668 DOI: 10.1063/1.1510279

669
670 Sarmiento, J. L., and Gruber, N. (2006), Ocean biogeochemical dynamics, Princeton University Press,
671 526 pp.

672
673 Sasse, T. P., McNeil, B. I., and Abramowitz, G. (2013a), A new constraint on global air-sea CO2
674 fluxes using bottle carbon data, Geophysical Research Letters, 40, 1594-1599, DOI:
675 10.1002/grl.50342

676
677 Sasse, T. P., McNeil, B. I., and Abramowitz, G. (2013b), A novel method for diagnosing seasonal to
678 inter-annual surface ocean carbon dynamics from bottle data using neural networks, Biogeosciences,
679 10, 4319-4340, DOI: 10.5194/bg-10-4319-2013

680
681 Schuster, U., Watson, A. J., Bates, N. R., Corbiere, A., Gonzalez-Davila, M., Metzl, N., Pierrot, D.,
682 and Santana-Casiano, M. (2009), Trends in North Atlantic sea-surface fCO_2 from 1990 to 2006, Deep

683 Sea Research Part II: Topical Studies in Oceanography, 56, 620-629, DOI:
684 10.1016/j.dsr2.2008.12.011

685
686 Séférian, R., Bopp, L., Gehlen, M., Orr, J., Ethé, C., Cadule, P., Aumont, O., Salas y Mélia, D.,
687 Voldoire, A., and Madec, G. (2013), Skill assessment of three earth system models with common
688 marine biogeochemistry, Climate Dynamics, 40, 2549-2573, DOI: 10.1007/s00382-012-1362-8

689
690 Shaw, E. C., Munday, P. L., and McNeil, B. I. (2013), The role of CO2 variability and exposure time
691 for biological impacts of ocean acidification, Geophysical Research Letters, 40, 4685-4688, DOI:
692 10.1002/grl.50883

693
694 Steinacher, M., Joos, F., Frölicher, T. L., Plattner, G. K., and Doney, S. C. (2009), Imminent ocean
695 acidification in the Arctic projected with the NCAR global coupled carbon cycle-climate model,
696 Biogeosciences, 6, 515-533, DOI: 10.5194/bg-6-515-2009

697
698 Takahashi, T., Sutherland, S. C., Wanninkhof, R., Sweeney, C., Feely, R. A., Chipman, D. W., Hales,
699 B., Friederich, G., Chavez, F., Sabine, C. L., Watson, A., Bakker, D. C. E., Schuster, U., Metzl, N.,
700 Yoshikawa-Inoue, H., Ishii, M., Midorikawa, T., Nojiri, Y., Körtzinger, A., Steinhoff, T., Hoppema,
701 M., Olafsson, J., Arnarson, T. S., Tilbrook, B., Johannessen, T., Olsen, A., Bellerby, R. G. J., Wong,
702 C. S., Delille, B., Bates, N. R., and de Baar, H. J. W. (2009), Climatological mean and decadal change
703 in surface ocean pCO_2, and net sea-air CO_2 flux over the global oceans, Deep Sea Research Part II:
704 Topical Studies in Oceanography, 56, 554-577, DOI: 10.1016/j.dsr2.2008.12.009

705
706 Takahashi, T., Sutherland, S. C., Chipman, D. W., Goddard, J. G., Ho, C., Newberger, T., Sweeney,
707 C., and Munro, D. R. (2014), Climatological distributions of pH, pCO_2, total CO_2, alkalinity, and
708 $CaCO_3$ saturation in the global surface ocean, and temporal changes at selected locations, Marine
709 Chemistry, 164, 95-125, DOI: 10.1016/j.marchem.2014.06.004

710
711 Tjiputra, J. F., Olsen, A., Bopp, L., Lenton, A., Pfeil, B., Roy, T., Segschneider, J., Totterdell, I., and
712 Heinze, C. (2014), Long-term surface pCO_2 trends from observations and models, Tellus B, DOI:
713 10.3402/tellusb.v66.23083

714
715 Tupper, M., Tan, M. K., Tan, S. L., Radius, M. J., and Abdullah, S. (2011), ReefBase: a global
716 information system on coral reefs, http://www.reefbase.org,

717
718 Zahariev, K., Christian, J. R., and Denman, K. L. (2008), Preindustrial, historical, and fertilization
719 simulations using a global ocean carbon model with new parameterizations of iron limitation,
720 calcification, and N2 fixation, Progress in Oceanography, 77, 56-82, DOI:
721 10.1016/j.pocean.2008.01.007

722
723 Zweng, M. M., Reagan, J. R., Antonov, J. I., Locarnini, R. A., Mishonov, A. V., Boyer, T. P., Garcia,
724 H. E., Baranova, O. K., Johnson, D. R., D.Seidov, and Biddle, M. M. (2013), World Ocean Atlas
725 2013, Volume 2: Salinity, in, edited by: Levitus, S., and Mishonov, A., NOAA Atlas NESDIS 74, 39
726 pp.

727

728

Region	Zone[a]	RSE[b]	*N*[c]
Arctic Ocean	1	0.22	673
Sup-Polar North Atlantic	2	0.13	2380
Sub-Tropical North Atlantic	3	0.11	1205
Equatorial Atlantic	4	0.16	565
Sub-Tropical South Atlantic	5	0.12	527
Sub-Polar North Pacific	6	0.18	1541
Sub-Tropical North Pacific	7	0.15	1412
Equatorial Pacific	8	0.16	764
Sub-Tropical South Pacific	9	0.15	1353
Sub-Tropical North Indian	10	0.13	137
Equatorial Indian	11	0.13	481
Sub-Tropical South Indian	12	0.11	1340
Southern Ocean	13	0.10	2923
Subantarctic waters	14	0.11	1426
Global		**0.138**	**16727**

Table 1: Regional and global skill evaluation for our predicted Ω_{Ar} values (see Fig. S3 for map of spatial division).

[a] Corresponding geographical region in Fig. S3

[b] Residual Standard Error

[c] number of measurements

Model	Ocean Resolution	BGC model	Reference
CanESM2	0.9-1.4°	CMOC	Zahariev et al. (2008)
GFDL-ESM2G	0.3-1°	TOPAZ2	Dunne et al (2013)
HadGEM2-ES	0.3-1°	Diat-HadOCC	Palmer and Totterdell (2001)
IPSL-CM5A-LR	0.5-2°	PISCES	Aumont and Bopp (2006), Séférian et al. (2013)
IPSL-CM5A-MR	0.5-2°	PISCES	Aumont and Bopp (2006), Séférian et al. (2013)
MPI-ESM-MR	0.4°	HAMOCC5.2	Ilyina et al. (2013)

735

736 **Table 2:** Main characteristics of the 6 ESM used in this study.

RCP	Month-long onset mean±sd (RCP8.5)	Atmospheric CO_2 mean±sd (RCP8.5)	Corr. to RCP8.5	Number of 1°×1° grid cells
		North Pacific (30°N to 65°N)		
4.5	2057±24 (2040±15)	492±45 (501±61)	0.75	475
2.6	2022±21 (2022±15)	406±28 (428±46)	0.81	110
		North Atlantic (30°N to 70°N)		
4.5	2061±17 (2047±12)	505±36 (530±51)	0.86	37
2.6	2024±20 (2016±15)	415±39 (410±40)	0.88	3
		Southern Ocean (South of 45°S)		
4.5	2064±19 (2045±9)	505±30 (518±46)	0.75	2619
2.6	2033±15 (2030±8)	428±19 (450±29)	0.66	154

Table 3: Comparison between future aragonite projections under RCP4.5 and 2.6 relative to RCP8.5.

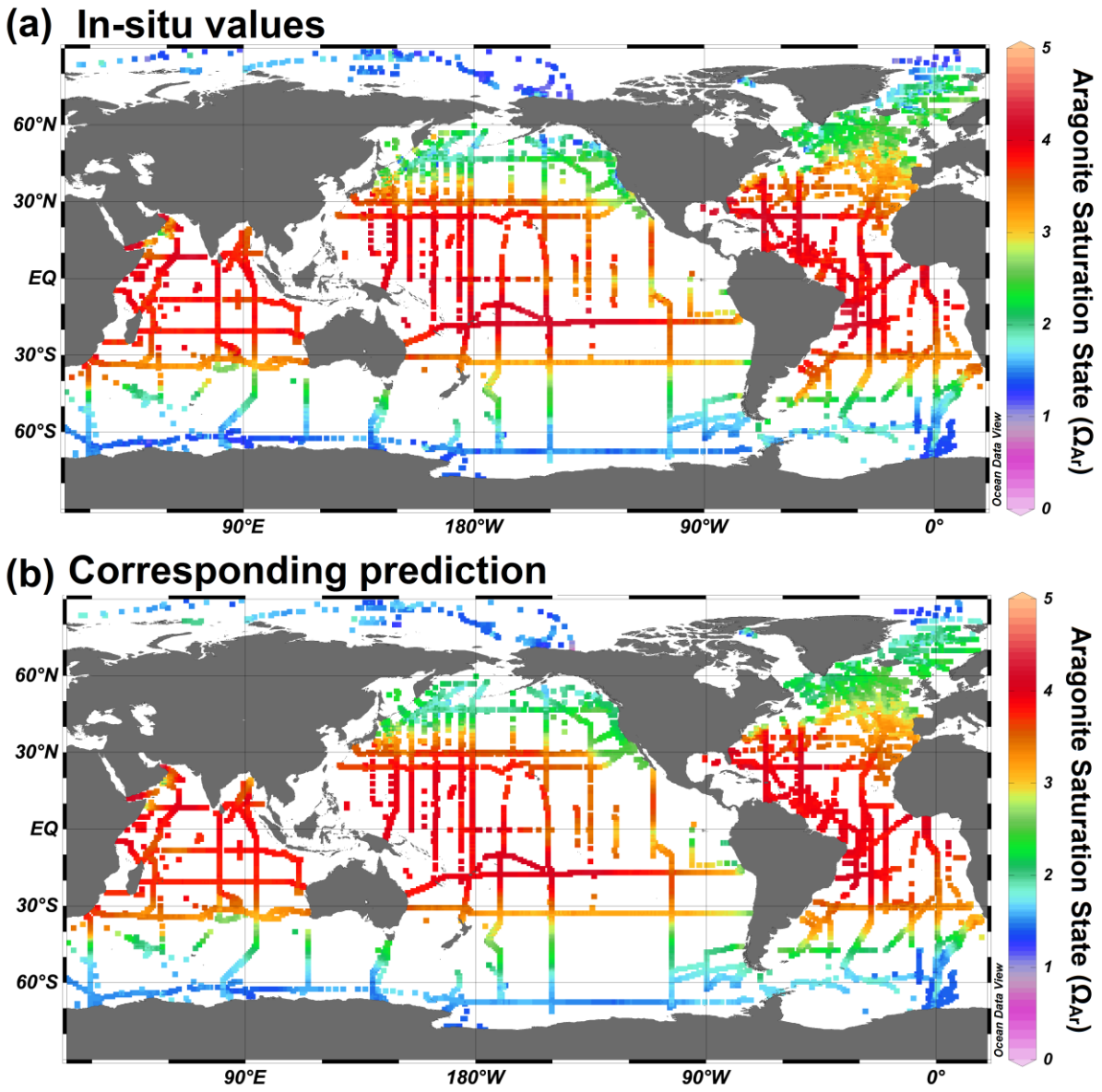

741

742 **Figure 1:** (a) In-situ Ω_{Ar} measurements normalised to the year 2000; (b) corresponding 1°×1°
743 Ω_{Ar} predictions for the same month and location for the nominal year for 2000 (see Supp. Fig.
744 S1 for monthly Ω_{Ar} distributions).

745

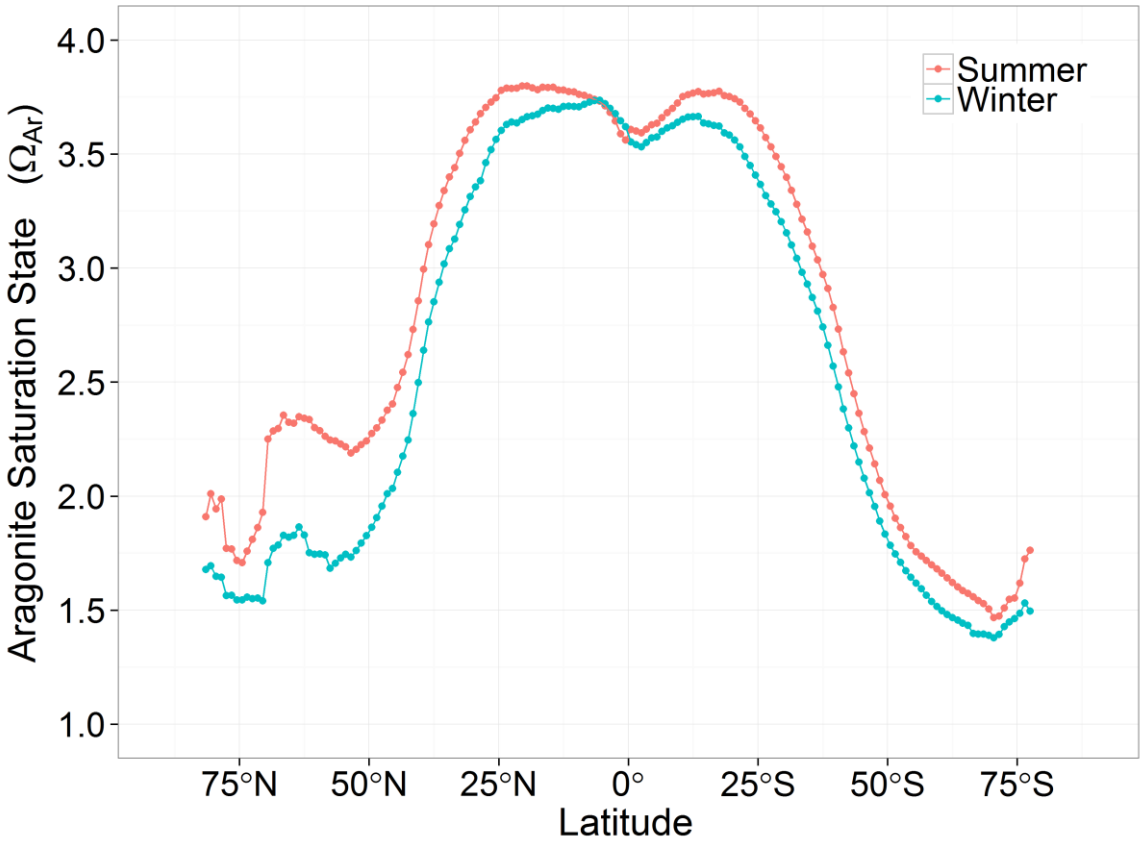

746

747 **Figure 2:** Zonal mean Ω_{Ar} predictions for winter and summer (joined dots). Summer and
748 winter months were defined as June through to August and December through to February for
749 Northern Hemisphere respectively, while Southern Hemisphere differed by 6 months.

750

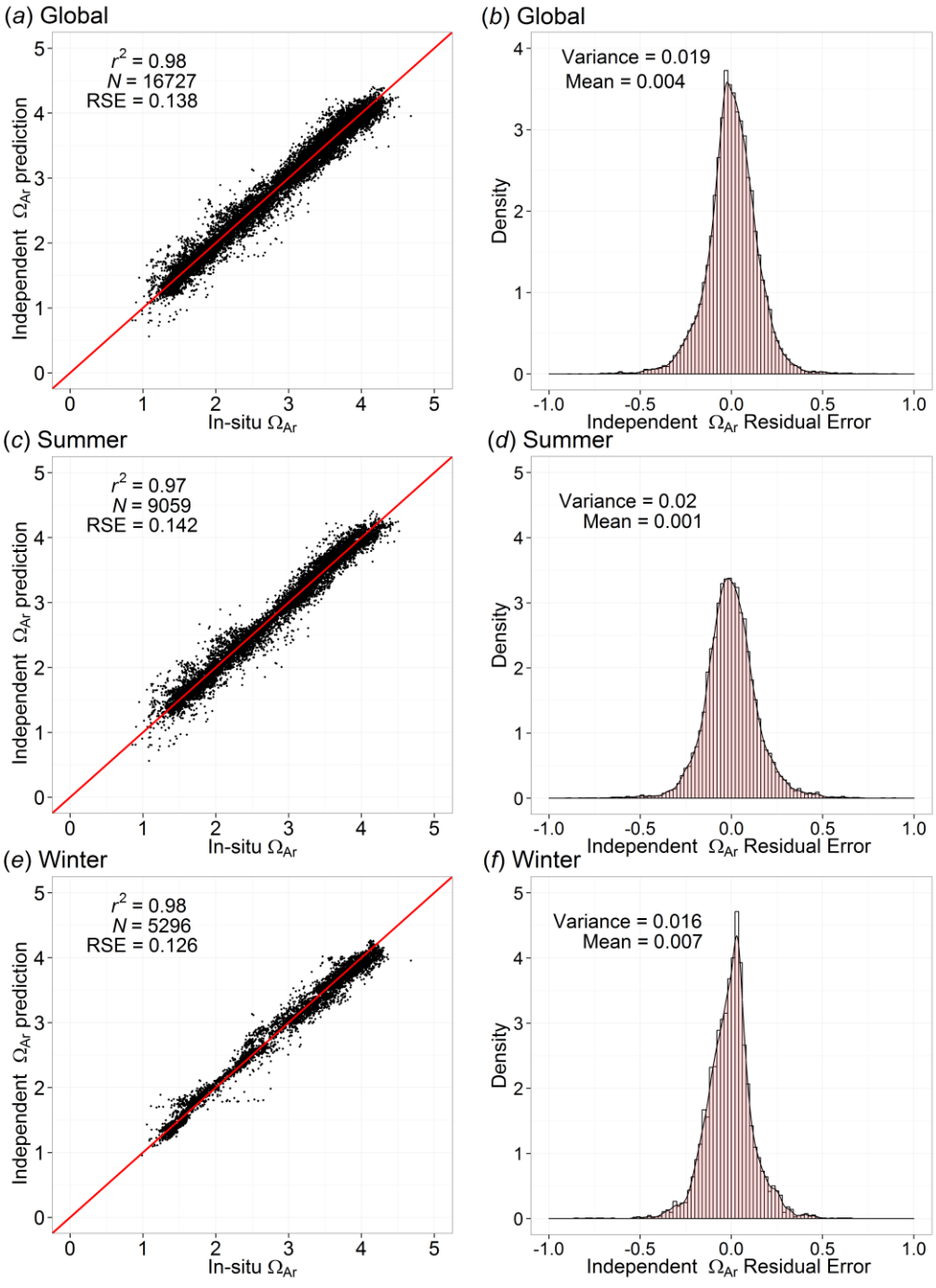

Figure 3: Statistical plots comparing global Ω_{Ar} values calculated via the network of in-situ C_T and A_T measurements and independently predicted C_T and A_T values of Sasse et al. (2013b). (a) Global independent predictions versus in-situ values, where the red line represents y = x relationship, (b) Global distribution of independent residual errors, (c,e) Winter and Summer independent predictions versus in-situ values, (d,f) Winter and Summer distribution of the independent residual errors. Summer and winter months were defined as May through to September and November through to March for Northern Hemisphere respectively, while Southern Hemisphere differed by 6 months.

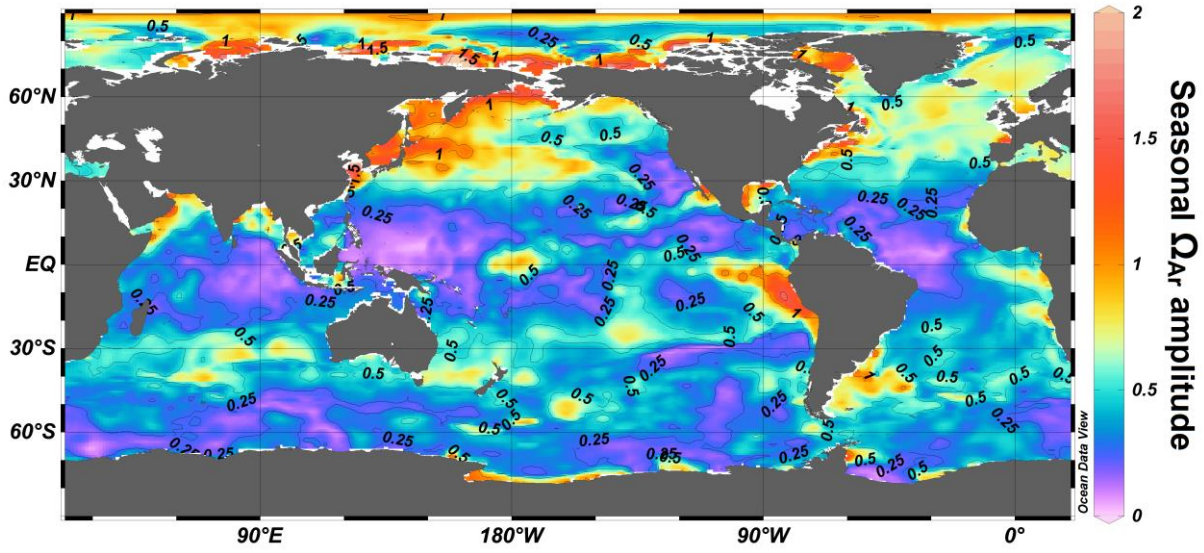

760

761 **Figure 4:** Seasonal Ω_{Ar} amplitudes for the nominal year of 2000. Seasonal amplitudes were
762 calculated as the maximum minus minimum monthly Ω_{Ar} values in each 1°x1° cell (see Fig.
763 S1 for monthly Ω_{Ar} distributions).

764

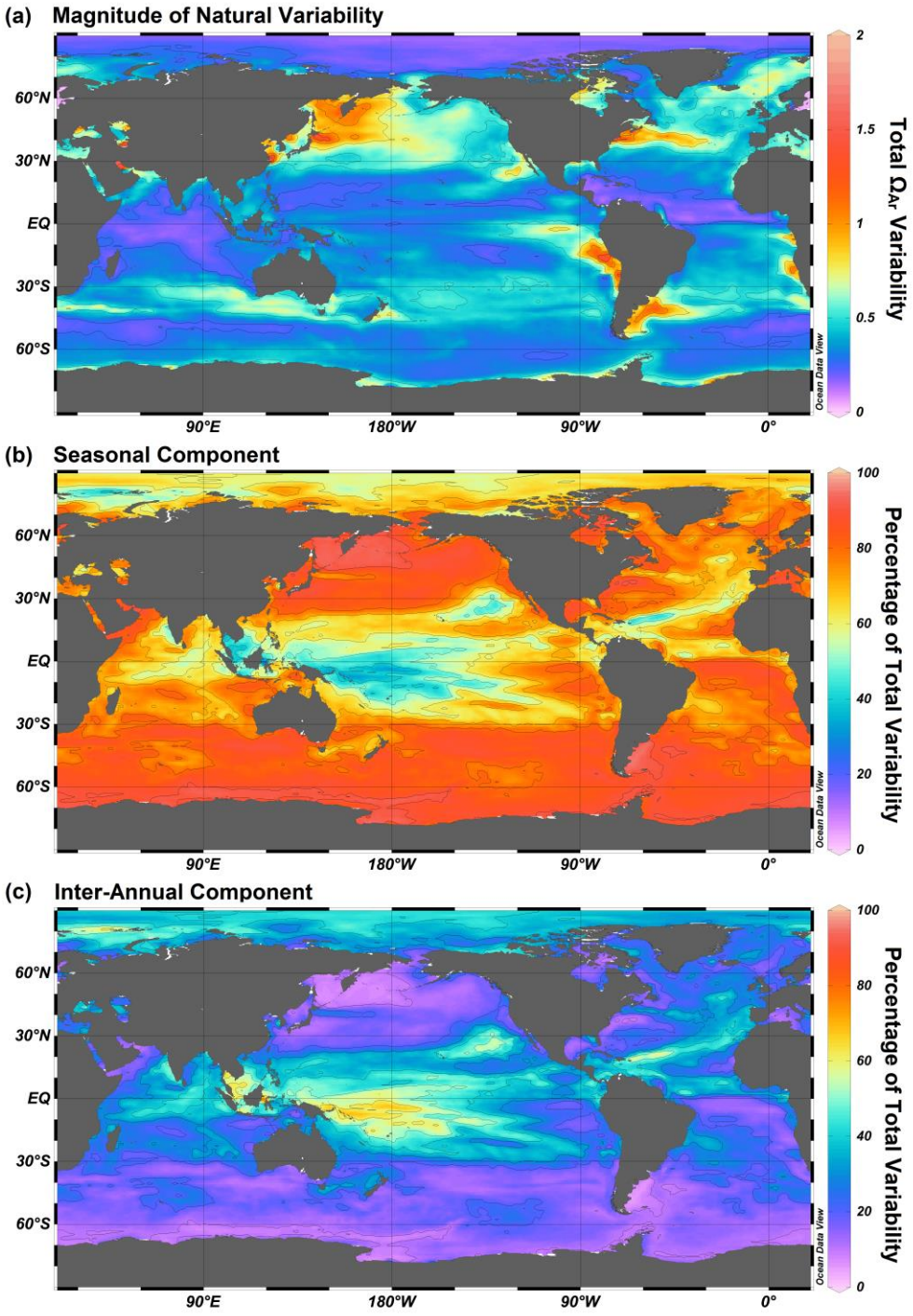

765

766 **Figure 5:** Model-based comparison of seasonal and inter-annual variability for ocean surface
767 Ω_{Ar}. (a) Total magnitude of variability as estimated from the ensemble of ESM. Here seasonal
768 variability was calculated as the mean seasonal amplitude between 2006 and 2016, while IAV
769 was calculated via the standard-deviation in de-trended annual mean projections between
770 2006 and 2100; (b) Relative contribution of seasonal variability to the total variability (in
771 percentage) (c) Relative contribution of inter-annual variability to the total variability (in
772 percentage).

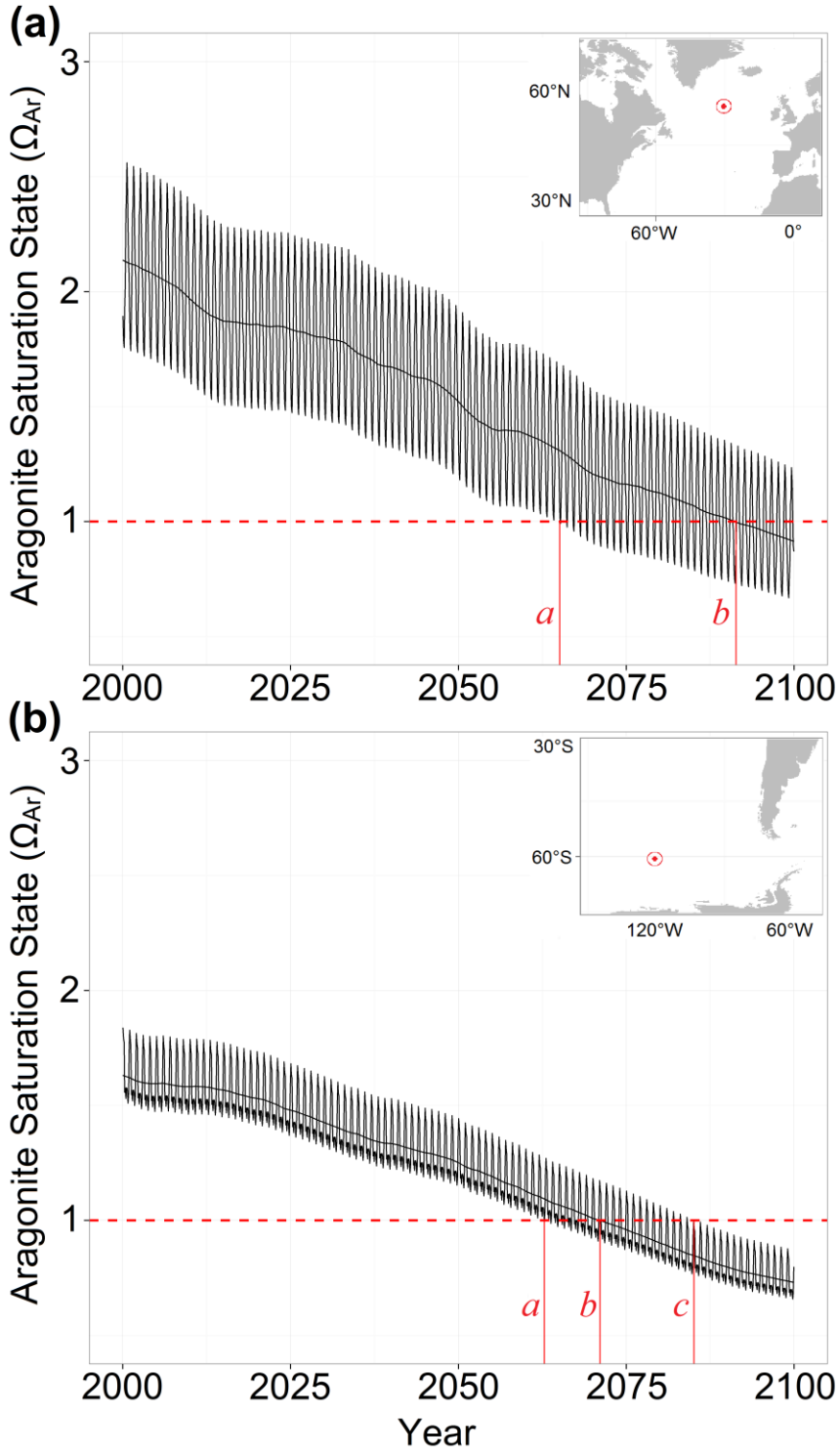

773

774 **Figure 6:** Future aragonite saturation states (Ω_{Ar}) at locations in the (a) North Atlantic and (b)
775 Southern Ocean under the *business-as-usual* scenario (RCP8.5). The influence of seasonal
776 variability accelerates under-saturation conditions by 27 and 8 years relative to annual-mean
777 estimates (black line) in the North Atlantic and Southern Ocean, respectively. The red points
778 *a*, *b*, and *c* denote the time when month-long, annual-mean and permanent under-saturation
779 occurs, respectively.

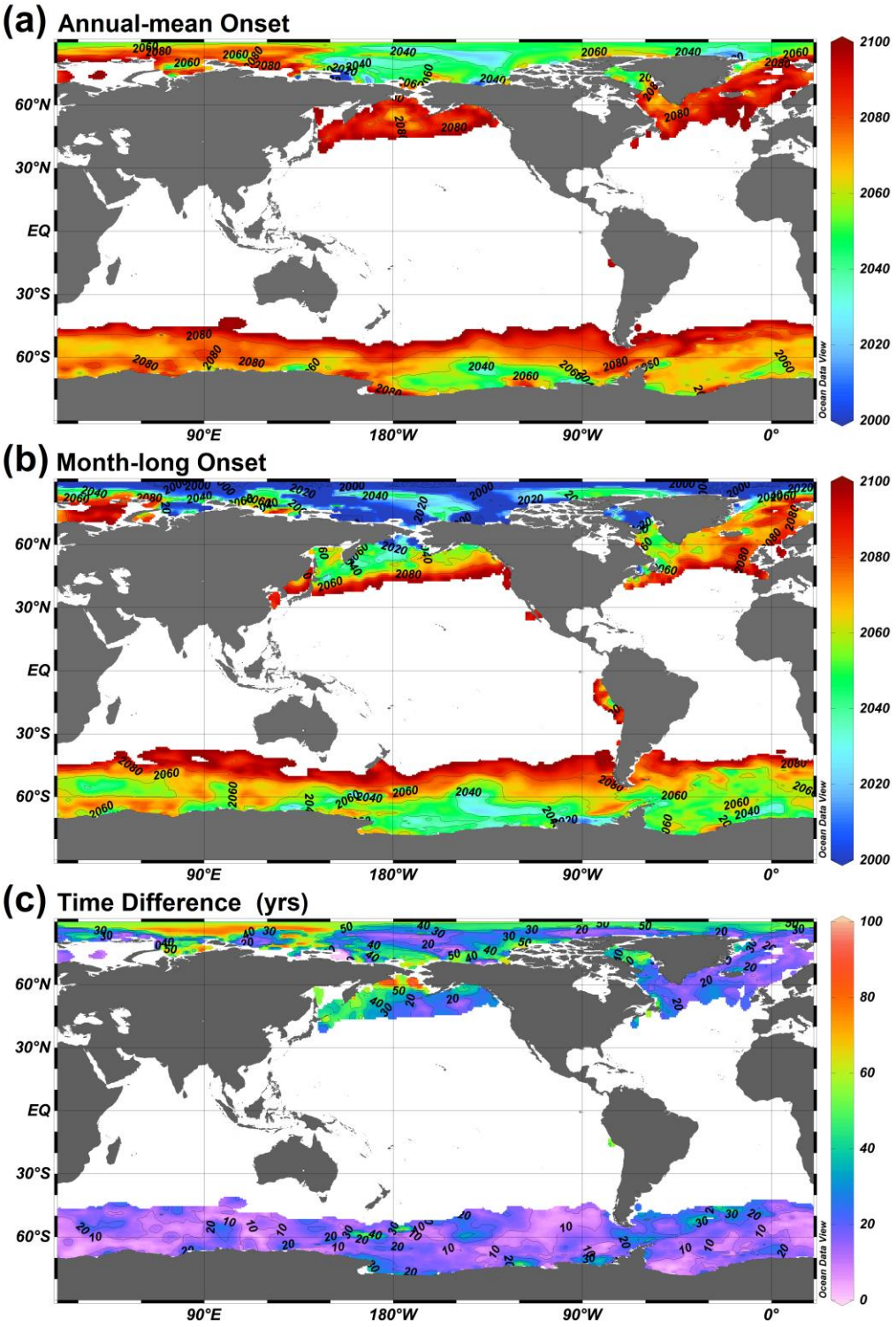

780

781 **Figure 7:**Estimated onset year for aragonite under-saturation under RCP8.5 for (a) annual-
782 mean and (b) one-month. (c) Time difference (years) between annual-mean and month-long
783 estimates.

784

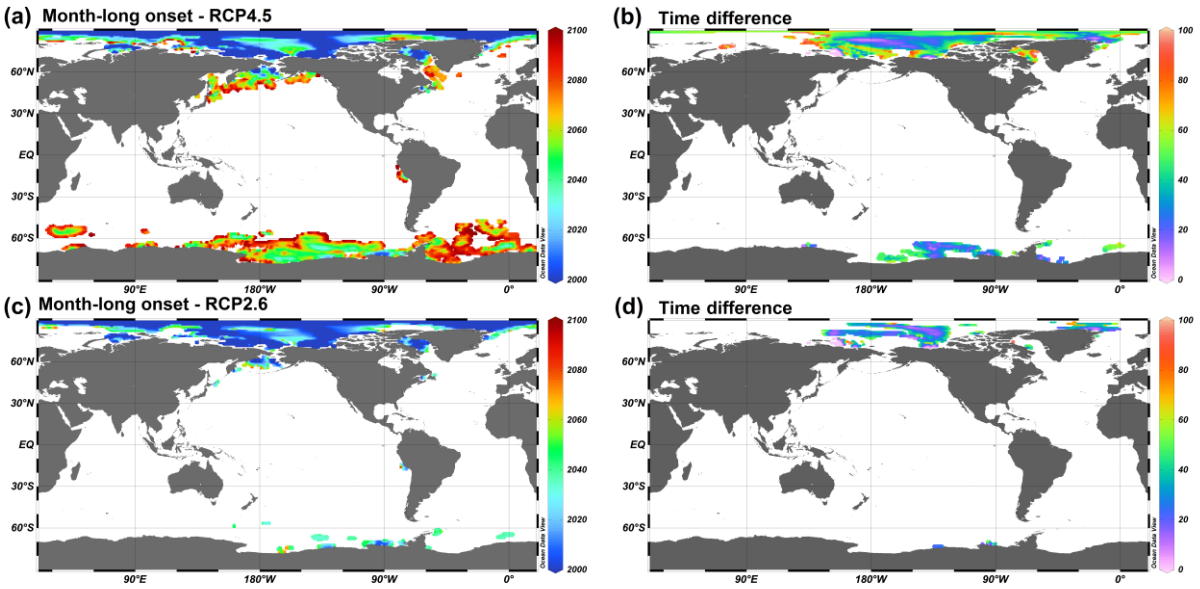

785

786 **Figure 8**: Onset year for month-long ocean surface aragonite under-saturation for (a) RCP4.5
787 and (c) RCP2.6. Time difference (years) between month-long and annual-mean surface
788 aragonite under-saturation onset under (b) RCP4.5 and (d) RCP2.6.

789

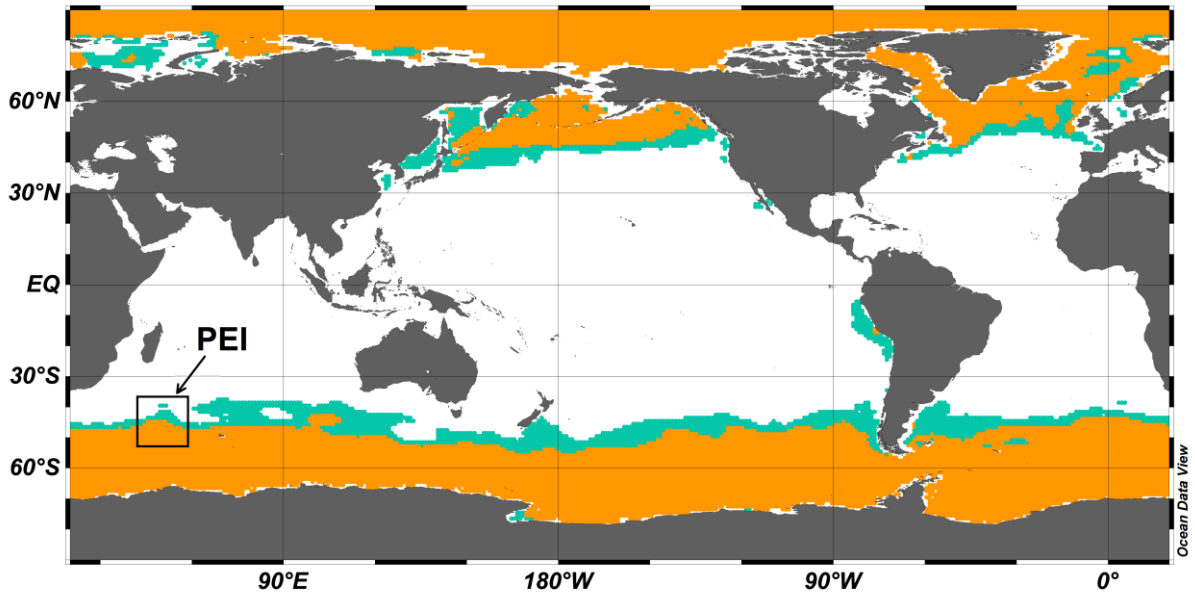

790

791 **Figure 9:** Surface area exposed to at least month-long (blue) and annual-mean (orange)
792 aragonite under-saturation in the year 2100 under RCP8.5. The blue region represents
793 ~23×10^6 km^2. The area labelled PEI represents the pteropod study region of Hunt et al. (2008)
794 around the Prince Edward Islands.